



OPEN ACCESS

EDITED BY

Yiqi Zhang,
Xi'an Jiaotong University, China

REVIEWED BY

Dumitru Mihalache,
Horia Hulubei National Institute for
Research and Development in Physics
and Nuclear Engineering (IFIN-HH),
Romania
Juanfen Wang,
Taiyuan University of Technology, China

*CORRESPONDENCE

Chong Liu,
chongliu@nwu.edu.cn

SPECIALTY SECTION

This article was submitted to Optics and
Photonics,
a section of the journal
Frontiers in Physics

RECEIVED 13 September 2022

ACCEPTED 10 October 2022

PUBLISHED 28 October 2022

CITATION

Wu Y-H, Liu C, Yang Z-Y and Yang W-L
(2022), Non-degenerate rogue waves
and multiple transitions in systems of
three-wave resonant interaction.
Front. Phys. 10:1043053.
doi: 10.3389/fphy.2022.1043053

COPYRIGHT

© 2022 Wu, Liu, Yang and Yang. This is
an open-access article distributed
under the terms of the [Creative
Commons Attribution License \(CC BY\)](#).
The use, distribution or reproduction in
other forums is permitted, provided the
original author(s) and the copyright
owner(s) are credited and that the
original publication in this journal is
cited, in accordance with accepted
academic practice. No use, distribution
or reproduction is permitted which does
not comply with these terms.

Non-degenerate rogue waves and multiple transitions in systems of three-wave resonant interaction

Yu-Han Wu^{1,2}, Chong Liu^{1,2,3*}, Zhan-Ying Yang^{1,2,3} and
Wen-Li Yang^{1,2,3,4}

¹School of Physics, Northwest University, Xi'an, China, ²Shaanxi Key Laboratory for Theoretical Physics
Frontiers, Xi'an, China, ³NSFC-SPTP Peng Huanwu Center for Fundamental Theory, Xi'an, China,
⁴Institute of Modern Physics, Northwest University, Xi'an, China

Non-degenerate rogue waves (RWs) and multiple transitions between RWs and solitons arising from vector three-wave resonant interaction are studied analytically and numerically. In contrast to the conventional degenerate RWs, such non-degenerate RWs consist of two fundamental RWs each with individual Lax spectral parameter. We show distinctive continuous transitions from bright (dark) RWs to four-petal RWs to dark (bright) solitons as the relative frequency between the wave components increases. The underlying mechanism of such processes is the non-monotonic variation of the energy exchanges between different components of the waves. We further reveal the transition dynamics of non-degenerate RWs. Finally, we confirm numerically the robustness of the transition dynamics in the presence of spontaneous modulation instability induced by white noise. Our results provide insights into the RW formation and the multiple transitions in systems with three-wave resonant interaction, and may offer the possibility of experimental observations in multi-component resonant processes.

KEYWORDS

three-wave resonant, non-degenerate rogue wave, state transition, modulation instability, energy exchange

1 Introduction

Three-wave resonant interaction (3WRI) enjoys a prominent status in various branches of nonlinear science [1–7]. It involves the simplest and lowest-order wave-wave coupling in weakly nonlinear and dispersive media [8–15]. The 3WRI has been extensively studied alongside with the development of nonlinear optics, since it applies to laser-plasma interaction [2], group-velocity pulse control [14, 16–19], ultrashort pulse train generation [7, 20], and frequency conversion [21].

The mathematical model that describes such interaction is commonly based on a coupled set of evolution equations [1, 22]. An integrable version of the latter was established in the early 1970s [1]. Just as the celebrated nonlinear Schrödinger equation (NLSE), an important point is that the integrable 3WRI system admits

various exact localized wave solutions in analytic form. These contain the resonant solitons [1, 13–15, 20] as well as the “breathing waves” such as breathers [23, 24] and rogue waves (RWs) [23–28]. Physically, these localized waves correspond to different nonlinear excitations [29, 30]. Recently, significant progress has been made on the 3WRI solitons and RWs. In particular, the 3WRI velocity-locked solitons have been confirmed in both theory and experiment [14, 15], and the existence of fundamental and high-dimensional RWs has been predicted in theory recently [25–27]. However, just as the scalar NLSE case [31–33], all existing 3WRI RWs are the conventional degenerate solutions. Namely, the RWs correspond to an identical spectral parameter of the associated Lax pair [25, 26, 28]. Recently, a new type of RWs—nondegenerate RWs—has been demonstrated in the coupled NLSEs accounting for the dynamics of vector waves in weak resonant processes [34]. Such non-degenerate RWs consist of different fundamental RWs each with individual Lax spectral parameter. This possibility arises from the internal integrable structure of the coupled NLSEs where the Lax pair is a multidimensional matrix. Just like the coupled NLSEs, the 3WRI equations also admit multidimensional (3 × 3) Lax matrix. Unlike the coupled NLSEs, the 3WRI equations are the fundamental model accounting for the dynamics of vector waves in strong resonant processes. It is therefore relevant to find out whether nondegenerate RWs exist in the 3WRI system.

On the other hand, as two different types of localized excitations, transitions between the 3WRI RWs and solitons remain completely unexplored. Transitions between different types of nonlinear waves in both the scalar and vector nonlinear systems have been a subject of extensive research. Recent studies have demonstrated that the transitions between RWs (or breathers) and solitons only exhibit a simple transition process—from bright (dark) RWs to bright (dark) solitons [35–37]. Namely, all these results are limited to a relatively simple single transition. It has been shown that such single transition describes a continuous process of RW elongation, which corresponds to the monotonic decay of modulation instability (MI) gain [36, 37].

In this paper, we demonstrate the existence of nondegenerate RWs in the 3WRI system, and reveal multiple transitions which are different from the single transition reported before [35–37]. The nondegenerate RWs consist of two fundamental RWs each with individual Lax spectral parameter. We present the existence diagram. We show that the multiple transitions are closely connected with the inherent energy exchange between different wave components of the 3WRI system. The latter is forbidden in the coupled NLSE case [38]. The robustness of all transition dynamics in the presence of spontaneous MI induced by white noise is confirmed numerically.

2 The three-wave resonant interaction system and rogue wave solutions

The 3WRI equations describing the propagation of three coupled waves in a weakly dispersive nonlinear medium [1, 8, 9], can be written as, in dimensionless form,

$$\begin{aligned} u_{1t} + c_1 u_{1z} &= u_2 u_3^*, \\ u_{2t} + c_2 u_{2z} &= -u_1 u_3, \\ u_{3z} &= (c_2 - c_1) u_1^* u_2, \end{aligned} \tag{1}$$

where $u_j(t, z)$, $j = 1, 2, 3$ are the slowly varying electric field envelopes of the three waves. If z is the evolution variable, then this system is the well-known 3WRI equation [1] where the three characteristic velocities are $1/c_1$, $1/c_2$, and 0; otherwise, if the evolution variable is t , this system models the nonlocal interaction of two waves, that is the transformation $u_3 = (c_2 - c_1) \int u_1^* u_2 dz$ in system (1) [39, 40]. In optics, the 3WRI Eq. 1 describes optical pulses with second-harmonic generation in a KTP crystal [14–16].

Due to the resonant conditions for the frequencies and momenta [8], the initial plane-wave background of Eq. 1 can be expressed as

$$\begin{aligned} u_1^{[0]} &= a_1 \exp[i(k_1 t + qz)], \\ u_2^{[0]} &= a_2 \exp[i(k_2 t - qz)], \\ u_3^{[0]} &= ia_3 \exp[i(k_2 - k_1)t - 2qz], \end{aligned} \tag{2}$$

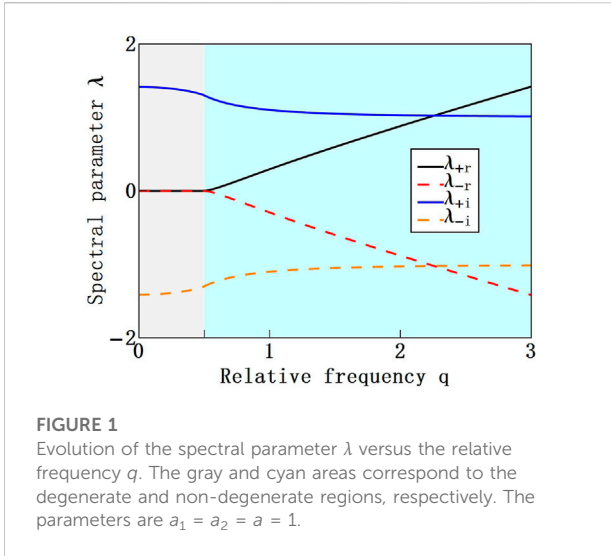
where

$$k_1 = -c_1 q - a_2^2 \delta, \quad k_2 = c_2 q - a_1^2 \delta, \quad a_3 = a_1 a_2 \delta, \quad \delta = \frac{c_2 - c_1}{2q},$$

with a_j , k_j , and q being the amplitudes, wavenumbers, and relative frequency of the vector plane-wave fields. The model (1) is integrable [1]. Namely, it admits various exact solutions. By solving the associated Lax pair (13), exact solutions describing localized nonlinear wave on the vector backgrounds (2) can be constructed by the Darboux transformation method [23]. The details are presented in Appendix. The first-order RW solutions $u_j^{[1]}$ of Eq. 1 are given by

$$\begin{aligned} u_1^{[1]} &= \left[1 + \frac{2i(\lambda^* - \lambda)\Psi_{11}^* \Psi_{21}}{|\Psi_{11}|^2 + a_1^2 |\Psi_{21}|^2 + a_2^2 |\Psi_{31}|^2} \right] u_1^{[0]}, \\ u_2^{[1]} &= \left[1 + \frac{2i(\lambda^* - \lambda)\Psi_{11}^* \Psi_{31}}{|\Psi_{11}|^2 + a_1^2 |\Psi_{21}|^2 + a_2^2 |\Psi_{31}|^2} \right] u_2^{[0]}, \\ u_3^{[1]} &= \left[1 + \frac{4q(\lambda^* - \lambda)\Psi_{21}^* \Psi_{31}}{|\Psi_{11}|^2 + a_1^2 |\Psi_{21}|^2 + a_2^2 |\Psi_{31}|^2} \right] u_3^{[0]}. \end{aligned} \tag{3}$$

Here, the expressions of Ψ_{11} , Ψ_{21} and Ψ_{31} as shown in the Supplementary Appendix S7.1. These solutions depend on the free parameters A_j and the spectral parameter λ . Solutions (3) describe RWs when one of A_j vanishes; otherwise, they describe the interaction between RWs and breathers when $A_j \neq 0$.



3 Non-degenerate rogue waves and transition dynamics

3.1 Spectral parameter analysis and characteristics of rogue waves

The spectral parameter λ in Eq. 3 is one of the complex roots of the discriminant condition:

$$(i\lambda M_1 - 9N_1)^2 + 4(\lambda^2 + 3M_1)(M_1^2 - 3i\lambda N_1) = 0, \quad (4)$$

where

$$M_1 = \lambda^2 + q^2 + a_1^2 + a_2^2, \quad (5)$$

$$N_1 = i[\lambda^3 - \lambda q^2 + a_1^2(\lambda - q) + a_2^2(\lambda + q)]. \quad (6)$$

For simplicity, we set here $a_1 = a_2 = a$. The spectral parameter λ is given explicitly by

$$\begin{cases} \lambda_{\pm} = \pm \frac{i}{4q}(\sqrt{-\Delta_1} - \sqrt{\Delta_2}), & |q| < a/2, \\ \lambda_{\pm} = \pm \frac{1}{4q}[\sqrt{\Delta_1} + i\sqrt{\Delta_2}], & |q| > a/2, \end{cases} \quad (7)$$

with

$$\begin{aligned} \Delta_1 &= 2q\sqrt{(2a^2 + q^2)^3 - \eta^2 - 18q^2(a^2 - q^2)}, \\ \Delta_2 &= 2q\sqrt{(2a^2 + q^2)^3 + \eta^2 + 18q^2(a^2 - q^2)}, \end{aligned}$$

and $\eta = a^2 - 4q^2$. The special case of $|q| = a/2$ has to be neglected to avoid singular solutions in Eq. 3.

We stress that, the spectral parameter λ plays a key role in the dynamics of localized waves. Namely, the imaginary part of λ determines the existence condition of the waves, while the real part determines the wave structures. In

particular, the sign of the imaginary part has no effect on the waveform; while the sign of the real part induces different waveforms.

Eq. 7 shows the variety of the spectral parameter λ . Namely, for any given initial parameters we have two spectral parameters λ_+ and λ_- . Such variety provides possibilities for new RW formation.

Figure 1 shows the evolution of the spectral parameter λ verse the relative frequency q . In the region $|q| < a/2$, both λ_+ and λ_- are purely imaginary ($\lambda_{+r} = \lambda_{-r} = 0$), and we have $\lambda_{+i} = -\lambda_{-i}$. Thus, RWs in this region are degenerate for any given a, q . Namely, $u_j^{[1]}(\lambda_+) = u_j^{[1]}(\lambda_-)$ when $|q| < a/2$. In contrast, in the region $|q| > a/2$, λ_+ and λ_- are complex, and $\lambda_+ = -\lambda_-$. This makes it possible to have two different RWs in the same parameter range, which is absent in previous results [25, 26]. Such two RWs are non-degenerate.

Figure 2 shows the amplitude distributions of RWs in the degenerate and non-degenerate regions, respectively. As shown in Figure 2A, RWs with λ_+ and λ_- in the degenerate region $|q| < a/2$ are identical, namely, $|u_j^{[1]}(\lambda_+)| = |u_j^{[1]}(\lambda_-)|$. Moreover, $|u_1^{[1]}|$ and $|u_2^{[1]}|$ feature standard bright RWs, while $|u_3^{[1]}|$ exhibits dark structure.

However, in the non-degenerate region, $|u_j^{[1]}(\lambda_+)|$ and $|u_j^{[1]}(\lambda_-)|$ are different not only in velocity but also in amplitude structure, as shown in Figure 2B. Specifically, $|u_j^{[1]}(\lambda_+)|$ exhibits vector four-petal-bright-bright RWs; while $|u_j^{[1]}(\lambda_-)|$ shows vector bright-four-petal-bright RWs.

Another remarkable result is that such RWs can exhibit the soliton structure when q is large. As shown in Figure 3, the vector RWs (Figure 3A) transform themselves to the vector solitons (Figure 3B) when q changes from 0.4 to 2. A comparison between the RWs (shown in Figure 2) and the solitons (shown in Figure 3) reveals a distinct type of transition between the bright (dark) RWs and the dark (bright) solitons. Examples are shown in the case of $u_{1,3}^{[1]}(\lambda_+)$ and $u_{2,3}^{[1]}(\lambda_-)$. This transition dynamics is different from the conventional transitions between bright (dark) RWs and bright (dark) solitons reported before [35–37].

3.2 Multiple transition of fundamental rogue waves

To better understand the transitions shown above, we focus our attention on $u_1^{[1]}(\lambda_+)$ with different frequencies. Figure 4 highlights the transition characteristics with the parameter variation from $q = 0$ to $q = 2$. The extremum of the amplitude profiles (at $z = -2.35$) versus the frequency are shown in Figure 4A. The maximum amplitude corresponds to the red and yellow curves, and the minimum amplitude is represented by the blue solid and dashed curves. The labels in Figure 4A correspond to the amplitude distributions of RWs in Figure 4B.

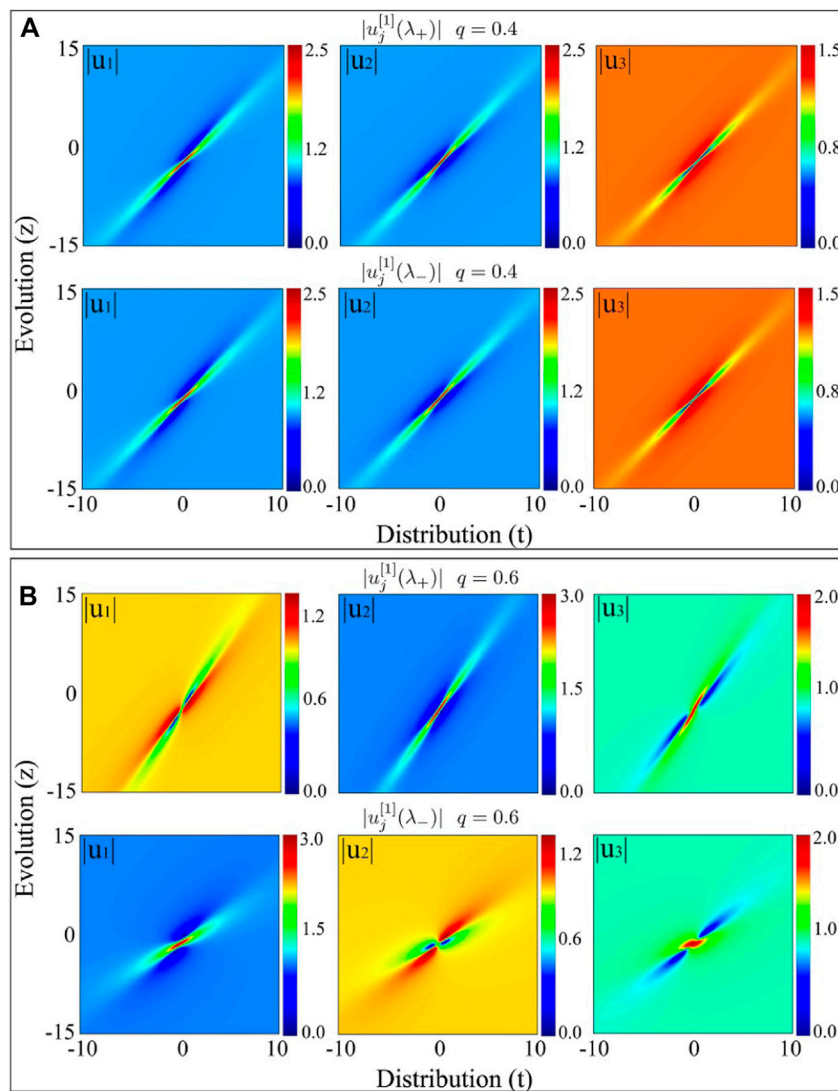


FIGURE 2 Amplitude distributions of RWs $|u_j^{[1]}(\lambda_+)$, $|u_j^{[1]}(\lambda_-)$ in the degenerate (A) and non-degenerate (B) regions. (A) RWs with $q = 0.4$ and (B) RWs with $q = 0.6$. The other parameters are $a_1 = a_2 = 1$, $c_1 = 1$, $c_2 = 2$, $A_1 = A_2 = 1$, and $A_3 = 0$. The spectral parameters λ_{\pm} are calculated by Eq. 7.

As can be seen, the structure of RWs is at first compressed then elongated with a continuously decreasing amplitude $|u_1^{[1]}(\lambda_+)$ as q increases. Finally, the RW is transformed into a soliton-like wave. The corresponding localization increases at first and then decreases.

Clearly, this transition process (a bright RW to a dark soliton) contains multiple wave states, namely bright RW [Figure 4 (b1)], four-petal RW [Figure 4 (b4)] and dark soliton [Figure 4 (b6)]. This stands in sharp contrast to the simple single transition reported before [35–37].

3.3 Non-degenerate second-order rogue waves

As shown in Section 3.1, for any given parameters in the non-degenerate region, there exist two different RWs. Let us consider whether such two RWs can coexist in the same plane wave. To answer this question, we proceed to construct the second-order RW solution in the non-degenerate region. The details are given by Supplementary Appendix S7.2. The solution is obtained by using the second-order iteration of the Darboux transformation with two

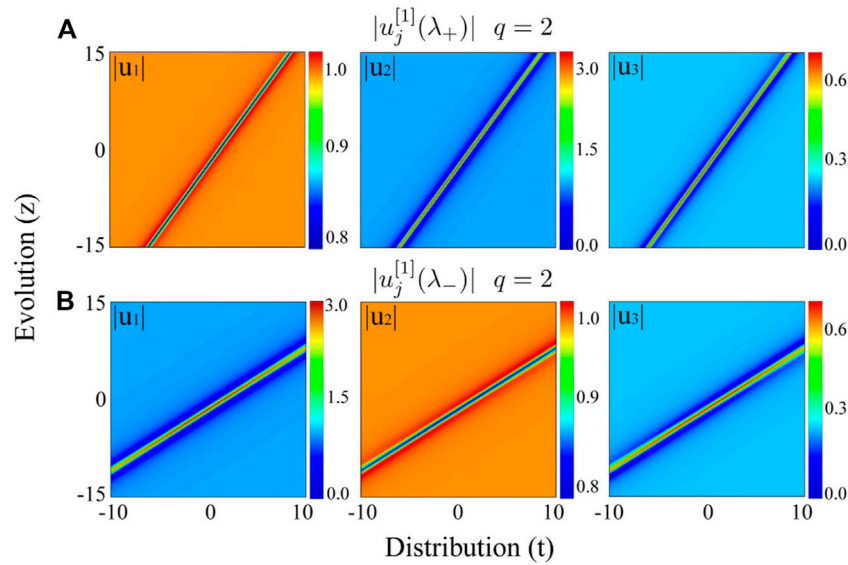


FIGURE 3
Amplitude distributions of solitons $|u_j^{[1]}(\lambda_+)|, |u_j^{[1]}(\lambda_-)|$ in the non-degenerate regions of $q = 2$. (A) Solitons with λ_+ and (B) solitons with λ_- . Other parameters are the same as in Figure 2.

spectral parameters $\{\lambda_+, \lambda_-\}$. Each spectral parameter corresponds to a RW. Thus, this solution describes the dynamics of the non-degenerate second-order RW. This higher-order RW solution is different from the degenerate multi-RWs presented before [25, 26].

Figure 5 shows the characteristics of non-degenerate second-order RWs with different q . To better analyze the variation of each RW structure, we have separated the RWs by the relative separations in both z and t , i.e., $z_1 = z - 1, t_1 = t + 1, z_2 = z + 1, t_2 = t - 1$. As can be seen from the figure, the second-order RWs (Figures 5A,B) have two different fundamental RWs. In particular, such two RWs can both transform into two solitons (Figure 5C). Interestingly, in either $u_1^{[2]}$ or $u_2^{[2]}$ component, two different types of transitions appear simultaneously in the same wave component. One is the multiple transition from bright RW to four-petal RW then to dark soliton; another is the single transition from bright RW to bright soliton.

4 Mechanism explanation

In previous results, the mechanism of single state transitions is explained well by the MI analysis [35–37]. To better understand the multiple transition, we use here the combination analysis of the MI and the energy exchange between different wave components. The latter is an important physical quantity in 3WRI system that can be

monitored in experiments. Such combination provides a solid interpretation for the transition mechanism.

We first pay attention to the standard modulation (linear) stability analysis. Adding a small-amplitude Fourier modes to the plane-wave solutions, we obtain

$$u_j = u_j^{[0]} \{ 1 + f_j e^{i\Omega(t-\mu x)} + g_j e^{-i\Omega(t-\mu^* x)} \}, \tag{8}$$

where f_j and g_j are small amplitudes, and the propagation parameters Ω and μ are assumed to be real and complex, respectively. A substitution of these perturbed plane-wave solutions into Eq. 1, followed by linearization yields the dispersion relation

$$\left[\left(\frac{a_1^2}{\mu c_1 - 1} + \frac{a_2^2}{\mu c_2 - 1} \right) \delta \mu - \frac{c_1 - c_2}{\delta} \right]^2 + \frac{4\mu a_2^2 (c_1 - c_2)}{\mu c_1 - 1} - \Omega^2 \mu^2 = 0. \tag{9}$$

Considering the condition of RW formation, namely, $\Omega \rightarrow 0$ [29, 30], we have the solutions of μ from Eq. 9 as follows

$$\mu_1 = \mu_r + i\mu_{i_1}, \quad \mu_2 = \mu_r + i\mu_{i_2}, \tag{10}$$

where μ_r denotes the real part, while μ_{i_1}, μ_{i_2} are the imaginary parts. For simplicity, we set $c_1 = 1$ and $c_2 = 2$. Their explicit expressions are given by

$$\mu_r = \begin{cases} \varrho_1 [\bar{\omega} + 3a^2 \sqrt{a\eta}], & |q| < a/2, \\ \varrho_1 [\bar{\omega} + 2aq\ell_1], & |q| > a/2, \end{cases}$$

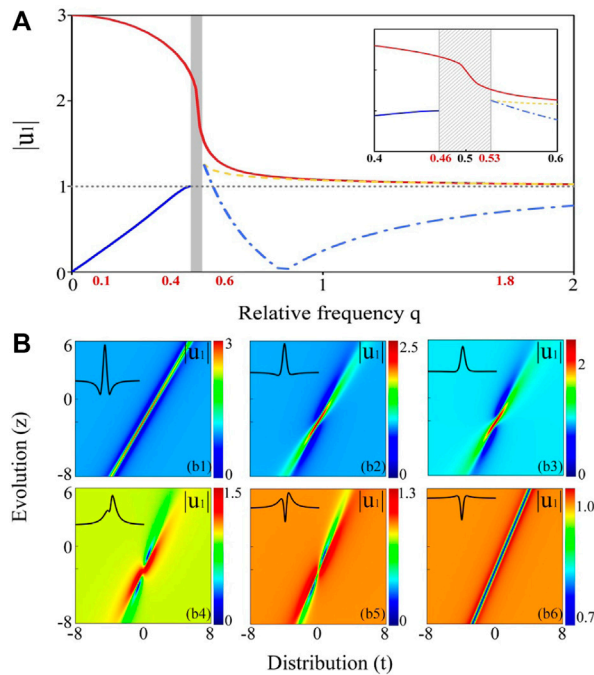


FIGURE 4 Characteristics of transitions on the certain range of frequency in the wave field $|u_1^{[1]}(\lambda_{\pm})|$. **(A)** Variation in the extremum of the amplitude profiles of RWs versus the frequency at $z = -2.35$, including the maximum $|u_{1max}^{[1]}|$ (red and yellow curves) and the minimum $|u_{1min}^{[1]}|$ (blue solid and dashed curves). There is only one maximum in the range $q \in (0.46, 0.53)$ (the gray area). Here the insert shows an enlargement of the gray area. Note that the amplitude profiles of RWs at $z = -2.35$ in this region have no minimum. As $q \geq 0.53$, there are two maximums and one minimum. **(B)** Amplitude distributions $|u_1^{[1]}|$ for (b1) $q = 0.1$, (b2) $q = 0.4$, (b3) $q = 0.46$, (b4) $q = 0.53$, (b5) $q = 0.6$, and (b6) $q = 2.5$. The insert curves in upper left correspond to the amplitude profiles at $z = -2.35$. Other parameters are the same as Figure 2.

and

$$\mu_{i_1} = \begin{cases} \pm \varrho_1 [2aq\sqrt{\Gamma_2 - \Gamma_1}], & |q| < a/2, \\ \pm \varrho_1 [3a^2\sqrt{-a\eta} - 2aq\ell_2], & |q| > a/2, \end{cases}$$

$$\mu_{i_2} = \begin{cases} \pm \varrho_1 [2aq\sqrt{\Gamma_1 + \Gamma_2}], & |q| < a/2, \\ \pm \varrho_1 [3a^2\sqrt{-a\eta} + 2aq\ell_2], & |q| > a/2, \end{cases}$$

where $\omega = 3\eta^2 + 18a^2q^2$, $\varrho_1 = [4\eta^2 + 5a^4 + 16a^2q^2]^{-1}$, $\Gamma_1 = (a^2 - 40q^2)\sqrt{a\eta}$, $\Gamma_2 = \eta^3 + 3a^2q^2(17a^2 - 32q^2)$, and $\ell_1 = [\frac{1}{2}\sqrt{\Gamma_2^2 - \Gamma_1^2 - \Gamma_2}]^{1/2}$, $\ell_2 = [\frac{1}{2}\sqrt{\Gamma_2^2 - \Gamma_1^2 + \Gamma_2}]^{1/2}$.

MI is described by the gain (growth rate). The latter is given by $G_{1,2} = |\text{Im}\{\mu_{1,2}\}| \neq 0$. It means that small-amplitude perturbations suffer MI and grow exponentially as $\exp(Gx)$ at the expense of pump waves.

Note that there are two different forms of the MI gain, namely $G = |\mu_{i_1}|$ and $G = |\mu_{i_2}|$. The existence condition of MI is consistent with the imaginary part of spectral parameter given by Eq. 7. As MI is regarded as the origin of RWs [29, 30], the two MI gains correspond to two different families of RWs.

On the other hand, the effective energy exchanges take place between the waves in different components. The effective energy has the form [25, 26].

$$E_j(\lambda_{\pm}) = \frac{1}{2} \int_{-\infty}^{+\infty} (|u_j^{[1]}(\lambda_{\pm})|^2 - |u_j^{[0]}|^2) dt. \tag{11}$$

For RWs with different spectral parameters λ_{\pm} , we have $E_j(\lambda_{\pm})$. In each case, one can verify that the effective energy obeys the relation $E_1 = E_3 = -2E_2$.

Figure 6A shows the variations of both the MI gain $G = |\mu_{i_1}|$, $G = |\mu_{i_2}|$ versus q . As can be seen, both two MI gains exhibit non-monotonic variation. Specifically, as q increases, MI gain increases first and reaches its peak at a certain $q = q_{max}$. It is given by $\partial|\mu_i|/\partial q = 0$. MI gain then decreases gradually and approaches to zero when q is relatively large. This process corresponds to the transition between RWs and solitons reported above.

However, one should note that the two MI gains admit different maximums. For $G = |\mu_{i_1}|$, we obtain $q_{max} = 0.46$; for $G = |\mu_{i_2}|$, we obtain $q_{max} = 0.6$. This indicates that the variations of the MI gains are asynchronous. To better understand the property

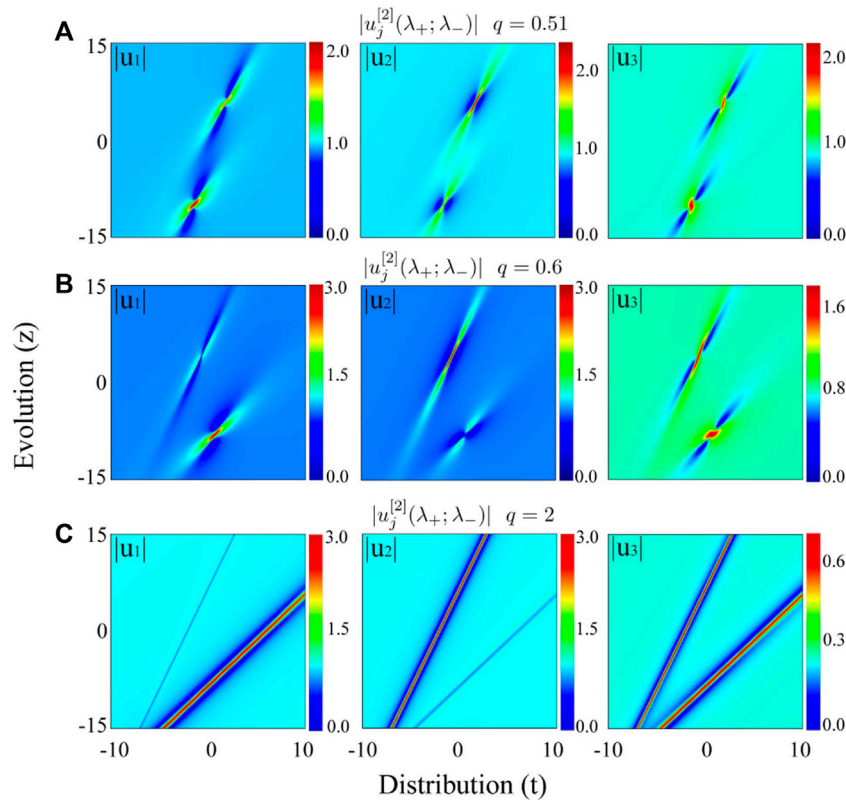


FIGURE 5

Amplitude distributions of non-degenerate second-order RWs, $|u_j^{[2]}(\lambda_+; \lambda_-)|$ with (A) $q = 0.51$, (B) $q = 0.6$, and (C) $q = 2$. From (A) to (C), one can see clearly the transitions between non-degenerate RWs and solitons. The exact second-order solutions as shown in the [Supplementary Appendix S7.2](#), other parameters are the same as Figure 2.

of MI, we further consider the characteristics of the effective energy of RWs.

Figure 6B shows the variations of the effective energy $E_j(\lambda_{\pm})$ versus q . All effective energies exhibit non-monotonic variation. For u_1 and u_3 , the effective energies $E_1(\lambda_{\pm})$ and $E_3(\lambda_{\pm})$ increase first and reach the maximums. They then decrease and approach to zero. However, the reverse process proceeds for $E_2(\lambda_{\pm})$ in u_2 wave component. This comes from the conservation law $E_1 + E_2 = E_2 + E_3$. A comparison between MI gains and the effective energy shows that the extreme point of $E_j(\lambda_+)$ is completely consistent with that of $G = |\mu_{i_1}|$; the extreme point of $E_j(\lambda_-)$ coincides with that of $G = |\mu_{i_2}|$. Thus, the multiple transition comes from the inherent non-monotonic variation of the effective energy in 3WRI system.

5 Numerical simulations

Finally, we discussed the robustness of the RWs and their transition dynamics. This can be done numerically by adding random noise to the initial states. Such perturbed initial states read

$$u_p = u_j(t, z = z_0)\{1 + m \text{ random}[-1, 1]\}, \quad (12)$$

where m is a small number denoting the amplitude of noise, $u_j(t, z = z_0)$ denotes the exact vector solution at a certain distance z_0 .

Figure 7 shows the numerical results of the fundamental RWs (a) and the transformed solitons (b). We take the initial states from the exact solutions $u_j^{[1]}(\lambda_+)(t, z_0 = -10)$ (shown in Figures 2A, 3A) perturbed by the noise amplitude $m = 0.001$. As can be seen from the figures, both RWs and solitons can suffer the random noises and be well reproduced. The following chaotic states appear as the result of the spontaneous MI.

Figure 8 shows the numerical results of the non-degenerate RWs (a) and the transformed solitons (b). The corresponding initial states are extracted from exact solutions $u_j^{[2]}(\lambda_+; \lambda_-)(t, z_0 = -15)$ (shown in Figures 5A,C) perturbed by the noise amplitude $m = 0.0001$. Despite being perturbed by random noises, the non-degenerate RWs and solitons are well reproduced. This result confirms the robustness of the non-degenerate RWs and solitons in 3WRI system.

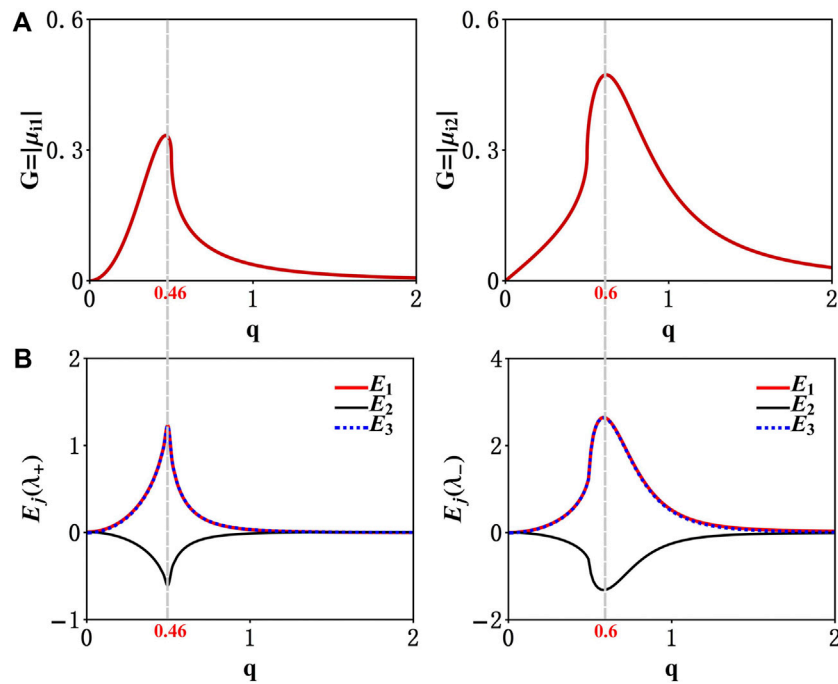


FIGURE 6 Non-monotonic variation of the MI gain (A) and effective energy (B) versus q , which can be obtained by Eqs 9, 11. Here the energy $E_j(\lambda_+)$ trend consistent with MI gain $G = |\mu_{11}|$, and the extreme point corresponds to the most localized structures RWs for $q = 0.46$. Another case of MI gain $G = |\mu_{12}|$ corresponding to the energy changes $E_j(\lambda_-)$ that reaches an extreme at $q = 0.6$.

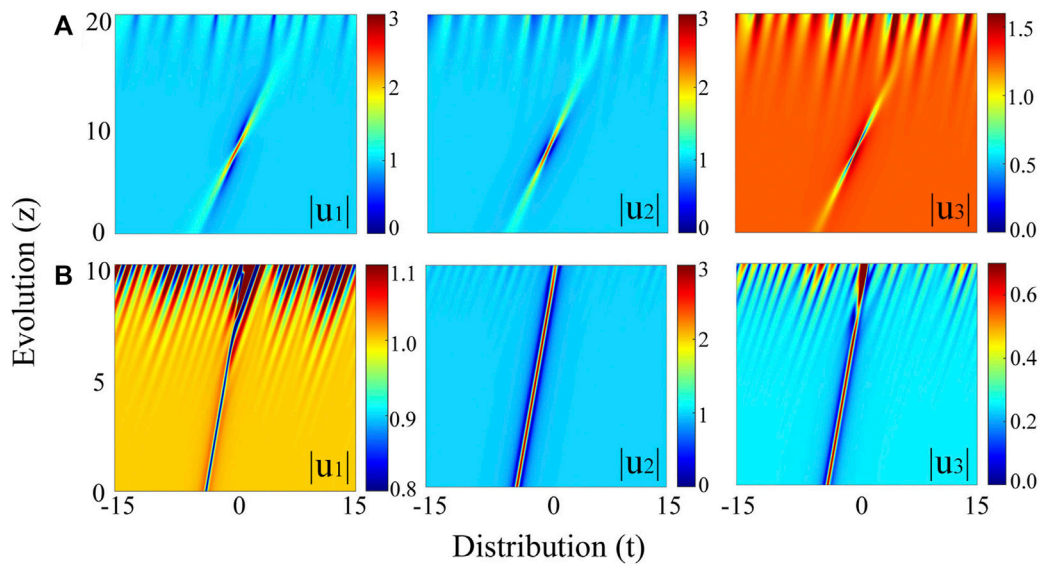


FIGURE 7 Numerical evolution of the transition between the fundamental RW (A) with $q = 0.4$ and soliton (B) with $q = 2$. The initial states are extracted from the exact solutions $u_j^{(1)}(\lambda_+)(t, z_0 = -10)$ (shown in Figures 2A, 3A) perturbed by the noise amplitude $m = 0.001$.

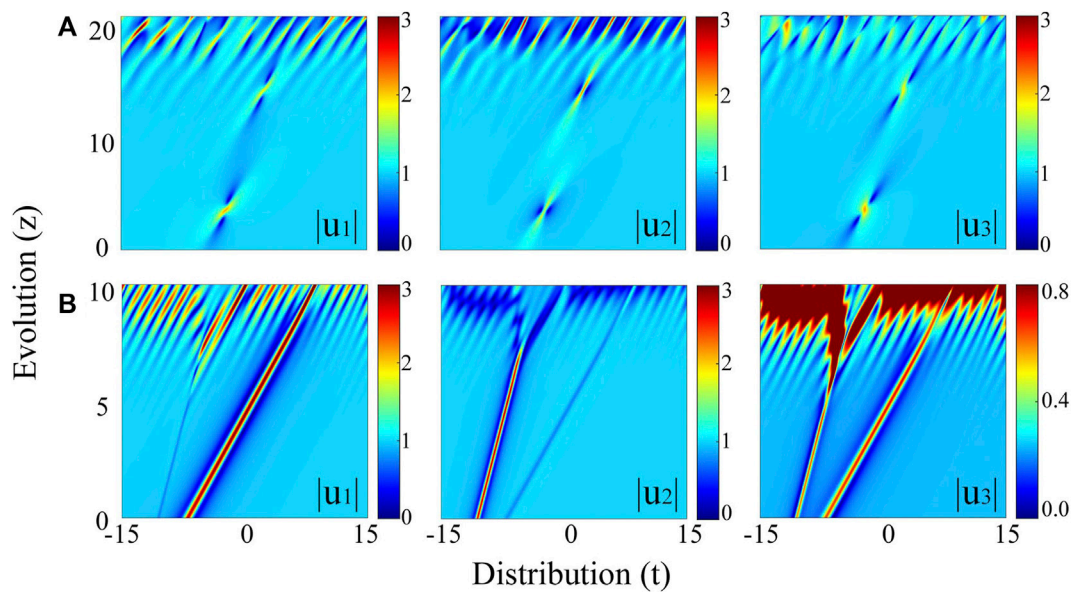


FIGURE 8

Numerical evolution of the transition between the nondegenerate RW (A) with $q = 0.4$ and (B) nondegenerate soliton with $q = 2$. The initial states are extracted from the exact solutions $u_j^{[z]}(\lambda_+; \lambda_-)(t, z_0 = -15)$ (shown in Figures 5A,C) perturbed by the noise amplitude $m = 0.0001$.

6 Conclusion

We demonstrated the existence, transition, formation mechanism, and stability of the nondegenerate RWs in the 3WRI system, which have not been reported before. The nondegenerate RWs consist of two fundamental RWs each with individual Lax spectral parameter. We present the existence diagram. We show that the multiple transitions are closely connected with the inherent energy exchange between different wave components of the 3WRI system, which is forbidden in the coupled NLSE systems. As the 3WRI equations are the fundamental model accounting for the dynamics of vector waves in strong resonant processes, our results could provide insights into the 3WRI RW formation, and may offer the possibility of experimental observations in multi-component resonant systems. On the other hand, the RW is just the limiting case of a breather with infinite period. Just like recent advances in nondegenerate breathers in coupled NLSEs [42, 43], we expect that 3WRI nondegenerate breathers will play a key role in understanding wave dynamics in strong resonant processes.

Data availability statement

The raw data supporting the conclusions of this article will be made available by the authors, without undue reservation.

Author contributions

CL conceived the ideal and wrote the first version of the manuscript. Y-HW presented the exact solutions of nonlinear excitations. All authors contributed to the physical analysis and revision of the manuscript.

Funding

This work is supported by the NSFC (Grants Nos 12275213, 12175178, 12004309, 12022513, and 12047502), the Major Basic Research Program of Natural Science of Shaanxi Province (No. 2017KCT-12), and the Natural Science basic Research Program of Shaanxi Province (Grant No. 2022KJXX-71).

Conflict of interest

The authors declare that the research was conducted in the absence of any commercial or financial relationships that could be construed as a potential conflict of interest.

Publisher's note

All claims expressed in this article are solely those of the authors and do not necessarily represent those of their

affiliated organizations, or those of the publisher, the editors and the reviewers. Any product that may be evaluated in this article, or claim that may be made by its manufacturer, is not guaranteed or endorsed by the publisher.

References

- Zakharov VE, Manakov SV. The theory of resonance interaction of wave packets in nonlinear media. *Zh Exp Teor Fiz* (1975) 69:1654–73.
- Malkin VM, Shvets G, Fisch NJ. Fast compression of laser beams to highly overcritical powers. *Phys Rev Lett* (1999) 82(22):4448–51. doi:10.1103/physrevlett.82.4448
- Lamb KG. Tidally generated near-resonant internal wave triads at a shelf break. *Geophys Res Lett* (2007) 34(18):L18607. doi:10.1029/2007gl030825
- Burlak G, Koshevaya S, Hayakawa M, Gutierrez-D E, Grimalsky V. Acousto-optic solitons in fibers. *Opt Rev* (2000) 7(4):323–5. doi:10.1007/s10043-000-0323-3
- Aubourg Q, Antoine C, Peureux C, Arduin F, Sommeria J, Viboud S, et al. Three-wave and four-wave interactions in gravity wave turbulence. *Phys Rev Fluids* (2017) 2(11):114802. doi:10.1103/physrevfluids.2.114802
- Deike L, Berhanu M, Falcon E. Experimental observation of hydroelastic three-wave interactions. *Phys Rev Fluids* (2017) 2(6):064803. doi:10.1103/physrevfluids.2.064803
- Cerullo G, De Silvestri S. Ultrafast optical parametric amplifiers. *Rev scientific Instr* (2003) 74(1):1–18. doi:10.1063/1.1523642
- Degasperis A, Lombardo S. Multicomponent integrable wave equations: II. soliton solutions. *J Phys A: Math Theor* (2009) 42(38):385206. doi:10.1088/1751-8113/42/38/385206
- Degasperis A, Conforti M, Baronio F, Wabnitz S, Lombardo S. The three-wave resonant interaction equations: Spectral and numerical methods. *Lett Math Phys* (2011) 96(1):367–403. doi:10.1007/s11005-010-0430-4
- Franken PA, Hill AE, el Peters CW, Gabriel W. Generation of optical harmonics. *Phys Rev Lett* (1961) 7(4):118–9. doi:10.1103/physrevlett.7.118
- Armstrong JA, Bloembergen N, Ducuing J, Pershan PS. Interactions between light waves in a nonlinear dielectric. *Phys Rev* (1962) 127(6):1918–39. doi:10.1103/physrev.127.1918
- Zernike F, Jr, Berman PR. Generation of far infrared as a difference frequency. *Phys Rev Lett* (1965) 15(26):999–1001. doi:10.1103/physrevlett.15.999
- Ibragimov E, Allan S. Second-harmonic pulse compression in the soliton regime. *Opt Lett* (1996) 21(19):1582–4. doi:10.1364/ol.21.001582
- Baronio F, Conforti M, De Angelis C, Degasperis A, Andreana M, Vincent C, et al. Velocity-locked solitary waves in quadratic media. *Phys Rev Lett* (2010) 104(11):113902. doi:10.1103/physrevlett.104.113902
- Degasperis A, Conforti M, Baronio F, Wabnitz S. Stable control of pulse speed in parametric three-wave solitons. *Phys Rev Lett* (2006) 97(9):093901. doi:10.1103/physrevlett.97.093901
- Picozzi A, Haelterman M. Parametric three-wave soliton generated from incoherent light. *Phys Rev Lett* (2001) 86(10):2010–3. doi:10.1103/physrevlett.86.2010
- Conforti M, Baronio F, Degasperis A, Wabnitz S. Inelastic scattering and interactions of three-wave parametric solitons. *Phys Rev E* (2006) 74(6):065602. doi:10.1103/physreve.74.065602
- Taranenko YN, Kazovsky LG. Three-wave envelope solitons: Can the speed of light in the fiber be controlled. *IEEE Photon Technol Lett* (1992) 4(5):494–7. doi:10.1109/68.136498
- Taranenko NL, Kazovsky LG, Taranenko YN. Three-wave envelope solitons: Possibility of controlling the speed of light in fiber. *J Lightwave Technol* (1994) 12(7):1101–11. doi:10.1109/50.301801
- Baronio F, Conforti M, Degasperis A, Wabnitz S. Three-wave trapponic solitons for tunable high-repetition rate pulse train generation. *IEEE J Quan Electron* (2008) 44(6):542–6. doi:10.1109/jqe.2008.917970
- Conforti M, Baronio F, Degasperis A, Wabnitz S. Parametric frequency conversion of short optical pulses controlled by a cw background. *Opt Express* (2007) 15(19):12246–51. doi:10.1364/oe.15.012246
- Romanova NN, Yu Annenkov S. Three-wave resonant interactions in unstable media. *J Fluid Mech* (2005) 539:57–91. doi:10.1017/s0022112005005665
- Degasperis A, Lombardo S. Rational solitons of wave resonant-interaction models. *Phys Rev E* (2013) 88(5):052914. doi:10.1103/physreve.88.052914
- Zhang G, Yan Z, Wen XY. Three-wave resonant interactions: Multi-dark-dark-dark solitons, breathers, rogue waves, and their interactions and dynamics. *Physica D: Nonlinear Phenomena* (2018) 366:27–42. doi:10.1016/j.physd.2017.11.001
- Baronio F, Conforti M, Degasperis A, Lombardo S. Rogue waves emerging from the resonant interaction of three waves. *Phys Rev Lett* (2013) 111(11):114101. doi:10.1103/physrevlett.111.114101
- Chen S, Baronio F, Soto-Crespo JM, Grelu P, Conforti M, Wabnitz S. Optical rogue waves in parametric three-wave mixing and coherent stimulated scattering. *Phys Rev A (Coll Park)* (2015) 92(3):033847. doi:10.1103/physreva.92.033847
- Yang B, Yang J. Rogue waves in (2+1)-dimensional three-wave resonant interactions. *Physica D: Nonlinear Phenomena* (2022) 432:133160. doi:10.1016/j.physd.2022.133160
- Chen S, Baronio F, Soto-Crespo JM, Grelu P, Mihalache D. Versatile rogue waves in scalar, vector, and multidimensional nonlinear systems. *J Phys A: Math Theor* (2017) 50(46):463001. doi:10.1088/1751-8121/aa8f00
- Baronio F, Conforti M, Degasperis A, Lombardo S, Onorato M, Wabnitz S. Vector rogue waves and baseband modulation instability in the defocusing regime. *Phys Rev Lett* (2014) 113(3):034101. doi:10.1103/physrevlett.113.034101
- Zhao LC, Ling L. Quantitative relations between modulational instability and several well-known nonlinear excitations. *J Opt Soc Am B* (2016) 33(5):850–6. doi:10.1364/josab.33.000850
- Akhmediev N, Adrian A, Soto-Crespo JM. Fundamental rogue waves and their superpositions in nonlinear integrable systems. *Nonlinear Guided Wave Opt A Testbed Extreme Waves* (2017).
- Akhmediev N. Waves that appear from nowhere: Complex rogue wave structures and their elementary particles. *Front Phys* (2021) 8:612318. doi:10.3389/fphy.2020.612318
- Mihalache D. Localized structures in optical and matter-wave media: A selection of recent studies. *Rom Rep Phys* (2021) 73(2):403.
- Liu C, Chen SC, Yao X, Akhmediev N. Non-degenerate multi-rogue waves and easy ways of their excitation. *Physica D: Nonlinear Phenomena* (2022) 433:133192. doi:10.1016/j.physd.2022.133192
- Zhao LC, Li SC, Ling L. Rational w-shaped solitons on a continuous-wave background in the sasa-satsuma equation. *Phys Rev E* (2014) 89(2):023210. doi:10.1103/physreve.89.023210
- Liu C, Yang ZY, Zhao LC, Yang WL. State transition induced by higher-order effects and background frequency. *Phys Rev E* (2015) 91(2):022904. doi:10.1103/physreve.91.022904
- Liu C, Yang ZY, Zhao LC, Yang WL. Transition, coexistence, and interaction of vector localized waves arising from higher-order effects. *Ann Phys* (2015) 362:130–8. doi:10.1016/j.aop.2015.06.008
- Yang J. *Nonlinear waves in integrable and nonintegrable systems*. Philadelphia, Pennsylvania, USA: SIAM (2010).
- Degasperis A. Integrable nonlocal wave interaction models. *J Phys A: Math Theor* (2011) 44(5):052002. doi:10.1088/1751-8113/44/5/052002
- Borgna JP, Degasperis A, Fernando De Leo M, Rial D. Integrability of nonlinear wave equations and solvability of their initial value problem. *J Math Phys* (2012) 53(4):043701. doi:10.1063/1.3699358
- Liu C, Chen SC, Yao XK, Akhmediev N. Modulation instability and non-degenerate akhmediev breathers of manakov equations. *Chin. Phys. Lett.* (2022) 39:094201.
- Che WJ, Chen SC, Liu C, Zhao LC, Akhmediev N. Nondegenerate kuznetsov solitons of manakov equations and their physical spectra. *Physical Review A* (2022) 105(4):043526.
- Guo B, Ling L, Liu QP. Nonlinear Schrödinger equation: Generalized darboux transformation and rogue wave solutions. *Phys Rev E* (2012) 85(2):026607. doi:10.1103/physreve.85.026607

Supplementary material

The Supplementary Material for this article can be found online at: <https://www.frontiersin.org/articles/10.3389/fphy.2022.1043053/full#supplementary-material>